Aryl-CF3 Coupling from Phosphinoferrocene-Ligated Palladium(II) Complexes

Devin M. Ferguson,[†] James R. Bour,[†] Allan J. Canty,[¥] Jeff W. Kampf,[†] and Melanie S. Sanford*,[†]

†Department of Chemistry, University of Michigan, 930 North University Ave, Ann Arbor, MI 48109, USA *School of Natural Sciences - Chemistry, University of Tasmania, Hobart, Tasmania 7001, Australia

increasing sterics of ligands increasing rate of Ph–CF₃ reductive elimination

ABSTRACT: This Article describes a detailed investigation of ligand effects on Ph–CF₃ coupling from phosphinoferrocene-ligated $Pd^{II}(Ph)(CF_3)$ complexes. This study reveals that increasing the size of the phosphine substituents results in an enhanced rate of Ph–CF₃ coupling, with $(D'BPF)Pd(Ph)(CF_3)$ (D'BPF = 1,1'-bis(di-tert-butylphosphino)ferrocene) being the most reactive complex. The mechanism of Ph–CF₃ bond formation from both $(D'BPF)Pd(Ph)(CF_3)$ and $(D'PrPF)Pd(Ph)(CF_3)$ (D'PrPF = 1,1'-bis(di-tert-butylphosphino)ferrocene) was interrogated experimentally and computationally. These studies implicate a pathway involving concerted Ph–CF₃ bond-forming reductive elimination from the four-coordinate Pd^{II} centers. An alternative pathway involving α -fluoride elimination and subsequent PhF_2C -F coupling from $Pd^{II}(CF_2Ph)(F)$ intermediates was also evaluated, but was ruled out based on DFT as well as the independent synthesis and reactivity studies of $(D'PrPF)Pd(CF_2Ph)(F)$.

INTRODUCTION

Over the past 20 years, transition-metal catalyzed cross-coupling reactions between aryl halides and trifluoromethyl nucle-ophiles have received widespread attention. While a variety of copper-catalyzed methods have been developed, analogous Pd-catalyzed transformations remain much more limited. At The quest for palladium catalysts for arene trifluoromethylation has focused on the identification of ligands that promote the challenging aryl-trifluoromethyl bond-forming step of the catalytic cycle. To date only five ligands, Xantphos (A), dfmpe (B), RuPhos, BrettPhos (C), and tri-tert-butylphosphine (P'Bu3, D), have been identified that promote high-yielding aryl-CF3 coupling from palladium(II) centers (Figure 1).

$$\begin{array}{c} \textbf{L}_{n} \textbf{Pd} \\ \hline \\ \textbf{PCF}_{3} \\ \hline \\ \textbf{CF}_{3} \\ \hline \\ \textbf{CF}_{4} \\ \hline \\ \textbf{CF}_{5} \\ \hline \\ \textbf{CF}_{$$

Figure 1. Ligands that promote Ph–CF₃ coupling at Pd^{II} centers.

The efficacy of these ligands has been rationalized based on a combination of steric effects, electronic effects, and ligand denticity. For instance, the bidentate Xantphos ligand has an unusually wide bite angle (102.07°), which was proposed to be an

enabling feature for its unique reactivity.^{5,9} In contrast, bidentate dfmpe has a much smaller bite angle (84.12°); however, its trifluoromethyl substituents are believed to promote Ph–CF₃ coupling by withdrawing electron density from the Pd^{II} center as well as by participating in unfavorable electrostatic interactions with the σ -phenyl and CF₃ ligands.^{6,10} BrettPhos and RuPhos are hemilabile bidentate ligands that coordinate to Pd^{II} via a strong Pd–P bond and a weak Pd–O interaction. The hemilabile nature of the Pd–O interaction provides facile access to reactive three-coordinate Pd^{II} centers. ^{11,12,13} Finally, the large size of P'Bu₃ enforces a three-coordinate geometry at Pd^{II}, which is believed to lower the barrier for Ph–CF₃ coupling. ^{8,11,12,13}

The structural diversity of ligands A-D has precluded meaningful comparisons of the relative impact of steric effects, electronic effects, and ligand denticity/bite angle on aryl-CF₃ coupling between these systems. Even within a given ligand class, there are only two computational studies that have systemically explored the role of ligand properties on the barrier for aryl-CF₃ bond formation. In one example, Schoenebeck probed reductive elimination from LPd^{II}(Ph)(CF₃), where L = bidentate Xantphos and DPPE (1,2-bis(diphenylphosphino)ethane) derivatives. Her work concluded that the relative barriers for Ph-CF₃ coupling were primarily governed by changes in steric repulsions at the ground state relative to the transition state. 14 In a related theoretical study of Ph-CF₃ coupling from (Xantphos)Pd^{II}(Ph)(CF₃), Bakhmutov, Grushin, and Macgregor concluded that the presence of sterically large cis ligands was important for facilitating reductive elimination in this system. 15 Inspired by these computational studies, we sought to experimentally interrogate steric effects on Ph–CF₃ coupling using the highly modular and readily available phosphinoferrocene class of ligands. Phosphinoferrocene-ligated Pd^{II} complexes are well known to participate in numerous challenging reductive elimination reactions, including the formation of aryl–NR₂¹⁶ and aryl–OR¹⁷ bonds. We report herein that phosphinoferrocene-ligated Pd^{II}(Ph)(CF₃) complexes participate in Ph–CF₃ coupling reactions, and that the rates of these reactions vary dramatically as a function of the ligand structure. The mechanism of these transformations and origin of these ligand effects are studied in detail using a combination of experiment and DFT calculations. Ultimately, this work offers insights that can aid the design of new ligands for Pd-catalyzed aryl–trifluoromethyl cross-coupling reactions.

RESULTS AND DISCUSSION

Synthesis of Phosphinoferrocene-Ligated Pd^{II}(Ph)(CF₃) Complexes. The phosphinoferrocene complexes **1-3** were prepared by the reaction of the appropriate phosphine ligand with (TMEDA)Pd(Ph)(CF₃) (TMEDA = *N,N,N',N'*-tetramethylethylenediamine). As shown in equation 1, the phosphines 1,1'-bis(diethylphosphino)ferrocene (DEtPF), 1,1'-bis(diphenylphosphino)ferrocene (DPPF), and 1,1'-bis(disopropylphosphino)ferrocene (D'PrPF) displace TMEDA quantitatively upon heating at 80 °C to afford **1-3** in isolated yields ranging from 45-67%.

$$\begin{array}{c} \begin{picture}(10,0) \put(0,0){\line(1,0){100}} \put(0,0){\line(1,$$

In contrast, the 1,1'-bis(di-*tert*-butylphosphino)ferrocene D'BPF complex **4** could not be isolated under these conditions. Instead, the major product detected by ¹⁹F NMR spectroscopy from the reaction between (TMEDA)Pd(Ph)(CF₃) and D'BPF was PhCF₃. This result suggests that initial ligand exchange to generate **4** is followed by rapid Ph–CF₃ coupling at the temperature required for TMEDA ligand substitution (80 °C). To facilitate ligand exchange at lower temperature, we next examined a Pd^{II} precursor bearing labile monodentate 3-fluoropyridine ligands.⁶ The reaction of D'BPF with (3-fluoropyridine)₂Pd(Ph)(CF₃) at room temperature initially afforded an equilibrium mixture of **4** and (3-fluoropyridine)₂Pd(Ph)(CF₃). However, removal of the free 3-fluoropyridine under vacuum drove this equilibrium to afford analytically pure **4** in 90% isolated yield (eq. 2).

The X-ray crystal structures of complexes **1-4** are shown in Figure 2, and selected bond distances and angles are presented in Table 1. In all cases the Pd–P1 bond distance is 0.0126-0.0855 Å longer than the Pd–P2 bond distance, consistent with the larger trans influence of the σ -phenyl relative to the CF3 ligand. The C1–Pd–C2 bond angle becomes more acute with increasing size of the substituents at phosphorus, ranging from 84.83° in **1** to 79.36° in **4**. Complexes **1-3** are all square planar, with angles between the P1–Pd–P2 and C1–Pd–C2 planes between 0.67° and 2.09° . In contrast, the D'BPF ligand imparts a significant distortion to the square plane in **4**, with an angle of

27.46° between the P1–Pd–P2 and C1–Pd–C2 planes.²⁰ Additionally, the P–Pd bond distances in **4** are approximately 0.1-0.2 Å longer than those in **1-3**. At 2.478 Å and 2.564 Å, respectively, these represent the longest P–Pd bonds reported for a mononuclear bidentate phosphine-ligated Pd^{II} species.²¹ Furthermore, the C1–Pd–C2 bond angle (79.36°) is the most acute C–Pd–C bond angle reported for a Pd^{II} species containing two independent carbon ligands.²¹ Finally, the bite angle of D'BPF (103.15°) is among the widest for Pd^{II} complexes bound to two independent carbon ligands.²¹ Overall, these features suggest a relatively destabilized ground state structure for **4**.

Complexes **1-4** were also characterized by ¹H, ³¹P, and ¹⁹F NMR spectroscopy in C₆D₆ or CD₂Cl₂. At room temperature, the ³¹P NMR spectra of **1-3** show a doublet of quartets and a quartet of doublets (Figure 3a). The observed signals implicate the presence of two inequivalent phosphine ligands that are coupled to one another as well as to the CF₃ ligand. The ¹⁹F NMR spectra of **1-3** show a doublet of doublets for the CF₃ ligand, consistent with coupling to the two inequivalent phosphine ligands (Figure 3b). These solution spectroscopic data are consistent with the solid-state structures of **1-3**.

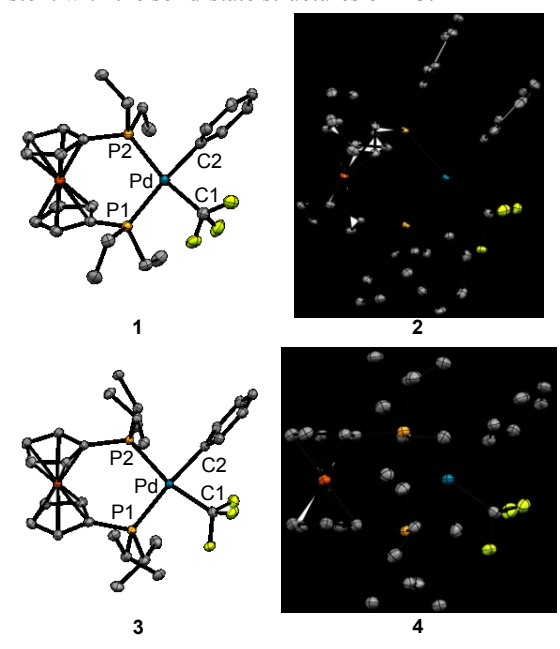


Figure 2. ORTEP diagrams for Pd^{II} complexes **1-4**. Hydrogen atoms have been omitted for clarity and ellipsoids are shown at 50% probability.

Table 1. Selected bond distances (Å) and selected bond angles (°) for **1-4**.

| complex | Pd-P1 | Pd-P2 | P1-Pd-P2 | C1-Pd-C2 |
|---------|-----------|-----------|-----------|-----------|
| 1 | 2.3732(8) | 2.3309(8) | 101.03(3) | 84.83(13) |
| 2 | 2.3670(5) | 2.3370(5) | 97.23(2) | 83.40(8) |
| 3 | 2.3959(6) | 2.3833(6) | 100.00(2) | 80.90(10) |
| 4 | 2.5639(7) | 2.4784(8) | 103.15(3) | 79.36(12) |

In contrast, complex 4 is fluxional at room temperature on the NMR timescale. ²² At 25 °C, the ³¹P NMR spectrum of 4 shows two broad resonances (Figure 3c), while the ¹⁹F NMR spectrum shows an apparent triplet (Figure 3d). Upon cooling the solution to –50 °C, the ³¹P NMR spectrum sharpens significantly (although the expected doublet of quartets and quartet of doublets do not completely resolve), and the ¹⁹F NMR spectrum shows

the expected doublet of doublets. These data suggest that exchange between the two phosphines in 4 is fast on the NMR timescale at room temperature. A proposed mechanism for this exchange involves initial dissociation of one phosphine to afford intermediate 4^{T} (i, Scheme 1), isomerization through a Y-complex (4^{Y}) to afford 4^{T} , and recoordination of the free phosphine (iv, Scheme 1).²³

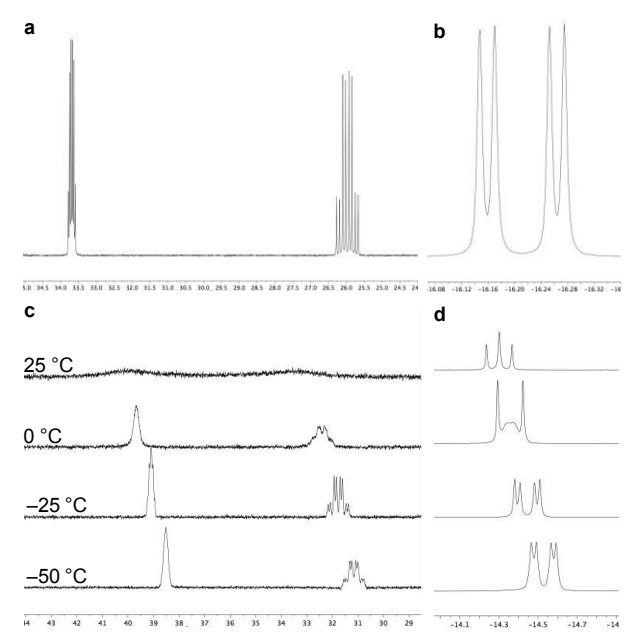


Figure 3. (a) ³¹P NMR spectrum for complex **3** at room temperature. (b) ¹⁹F NMR spectrum for complex **3** at room temperature. (c) Variable temperature (VT) ³¹P NMR spectrum of **4**. (d) VT ¹⁹F NMR spectrum of **4**.

Scheme 1. Proposed mechanism for phosphine exchange at 4.

Reductive Elimination from 1-4. Complexes **1-4** all participate in Ph–CF₃ coupling upon heating to 130 °C in *p*-xylene. Notably, 1 equiv of the phosphinoferrocene ligand was added to each reaction, to trap the Pd⁰ product and limit side reactions.²⁴ As shown in Figure 4, increasing the size of the phosphine substituent from ethyl (DEtPF) to phenyl (DPPF) to isopropyl (D'PrPF) to *tert*-butyl (D'BPF) results in a significant increase in the reaction rate. The least reactive DEtPF complex **1** afforded <5% of PhCF₃ after 50 min at 130 °C. The initial rate of reductive elimination from **2** (3.11 x 10⁻⁷ M/s) was approximately 1.3 times slower than that for **3** (3.98 x 10⁻⁷ M/s). Finally, the most reactive D'BPF complex **4** afforded complete conversion (and 75% yield of benzotrifluoride) after just 2 min under analogous conditions.

Further investigations were conducted to determine the optimal temperatures and times for PhCF₃ formation from 1-4. As

summarized in Table 2, the DEtPF complex 1 afforded 24% yield of PhCF₃ after 7 d at 130 °C. At this time, 57% of the starting material was consumed, suggesting that competing decomposition pathways are occurring in this system. In contrast, DPPF complex 2 yielded 89% of PhCF₃ after 36 h at 130 °C, while the D'PrPF complex 3 afforded 99% of PhCF₃ after 24 h at the same temperature. Finally, 4 produced benzotrifluoride in 82% yield after heating at 80 °C for 35 min. ^{25,26,27,28}

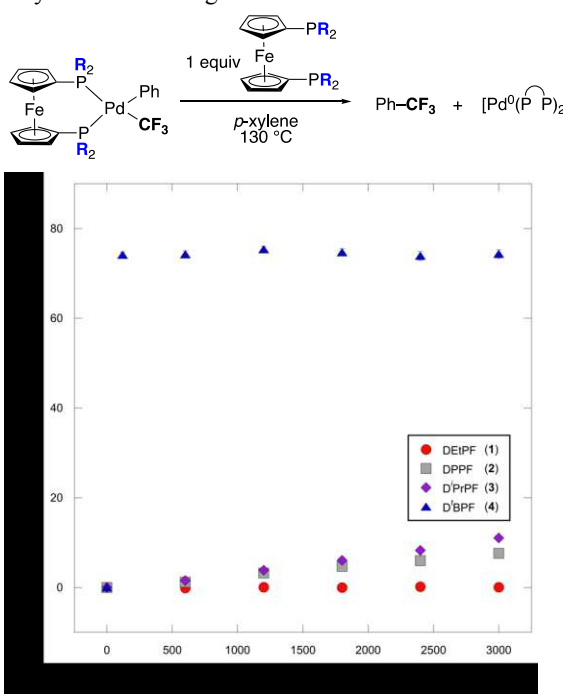
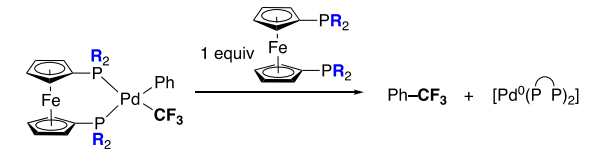


Figure 4. Time study of PhCF₃ formation from 1-4.

Table 2. Reductive elimination of benzotrifluoride from 1-4.



| complex | solvent | temp | time | yield PhCF ₃ |
|---------|----------|--------|--------|-------------------------|
| 1 | p-xylene | 130 °C | 168 h | 24% |
| 2 | p-xylene | 130 °C | 36 h | 89% |
| 3 | p-xylene | 130 °C | 24 h | 99% |
| 4 | C_6D_6 | 80 °C | 35 min | 82% |

Eyring plots were generated by evaluating the initial reaction rate of PhCF3 formation from 3 and 4 at different temperatures. As summarized in Table 3, reductive elimination from complex 3 proceeds with a ΔH^{\ddagger} of 29.7 kcal/mol, a ΔS^{\ddagger} of –5.8 eu, and a $\Delta G^{\ddagger}_{298}$ of 31.4 kcal/mol. The analogous reaction at 4 proceeds with a ΔH^{\ddagger} of 28.0 kcal/mol, a ΔS^{\ddagger} of +9.0 eu, and a $\Delta G^{\ddagger}_{298}$ of 25.3 kcal/mol. 29 The comparable ΔH^{\ddagger} values and relatively large difference in ΔS^{\ddagger} observed between 3 and 4 suggest that the faster rate of reductive elimination from 4 is largely entropically controlled.

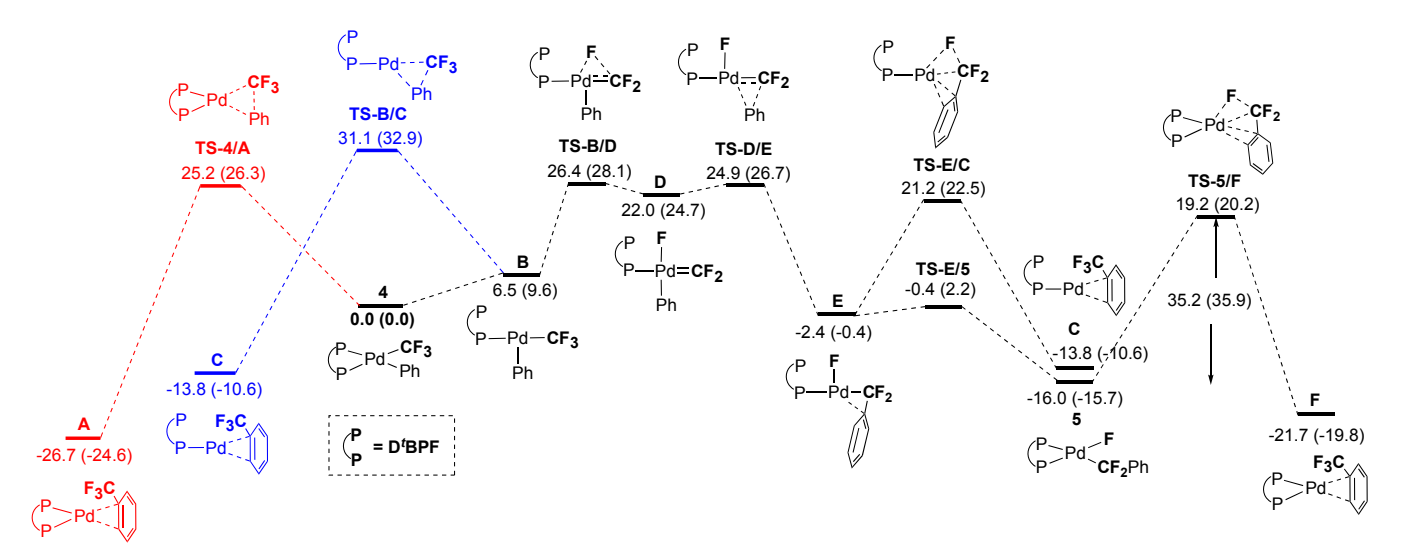


Figure 5. Energy profile for computed reactivity of (D'BPF)Pd(Ph)(CF₃) (4), illustrating pathway a (in red), pathway b (in blue), and pathway c (in black). A and F are conformers. Energies $\Delta G(\Delta H)$ in kcal/mol.

Table 3. Activation parameters for Ph–CF₃ coupling from complexes **3** and **4**.

$$\begin{array}{c} \begin{array}{c} \begin{array}{c} \begin{array}{c} \begin{array}{c} \\ \\ \\ \end{array} \end{array} \end{array} \begin{array}{c} \begin{array}{c} \\ \\ \end{array} \end{array} \begin{array}{c} \begin{array}{c} \\ \\ \end{array} \end{array} \begin{array}{c} \\ \end{array} \begin{array}{c} \\ \end{array} \begin{array}{c} \\ \end{array} \begin{array}{c} \\ \end{array} \end{array} \begin{array}{c} \\ \end{array} \end{array} \begin{array}{c} \\ \end{array} \end{array} \begin{array}{c} \\ \end{array} \end{array} \begin{array}{c} \\ \end{array} \begin{array}{c} \\ \end{array} \begin{array}{c} \\ \end{array} \begin{array}{c} \\ \end{array} \end{array} \begin{array}{c} \\ \end{array}$$

| | Experimental | | | DFT | | |
|---------|--|-------------------------------|----------------------|--|-------------------------------|--|
| complex | ΔG [‡] ₂₉₈ (kcal/mol) | ΔH [‡] (kcal/mol) | ΔS [‡] (eu) | ΔG [‡] ₂₉₈ (kcal/mol) | ΔH [‡] (kcal/mol) | |
| 3 | 31.4 ± 0.6 | 29.7 ± 0.6 | -5.8 ± 0.2 | 33.6 | 33.8 | |
| 4 | 25.3 ± 0.2 | 28.0 ± 0.1 | $+9.0\pm0.1$ | 25.2 | 26.3 | |

DFT Study of Ph-CF₃ Coupling from Phosphinoferrocene-Ligated Pd^{II}(Ph)(CF₃) Complexes. We next turned to DFT to investigate the mechanism of Ph-CF₃ coupling in these systems. 30,31,32,33,34,35,36 The literature suggests three possible pathways for this reaction. 13,15 The first (Scheme 2, pathway a) involves concerted coupling of the σ -phenyl and σ -CF₃ ligands from the bis-phosphine PdII starting material. The second involves pre-equilibrium dissociation of one arm of the bidentate phosphine followed by concerted reductive elimination from the three-coordinate intermediate **B** (Scheme 2, pathway b). Finally, the third involves α -fluoride elimination from 3-coordinate intermediate B to form difluorocarbene complex D, followed by α -phenyl migration to generate intermediate E (Scheme 2, pathway c). This PdII (difluorobenzyl)(fluoro) complex could then undergo PhF₂C-F coupling via either a 3- or 4coordinate pathway.

Our initial DFT studies focused on the D'BPF complex 4, and we first evaluated pathway a. Importantly, this pathway has been implicated in the literature for (Xantphos)Pd(Ph)(CF₃). ¹⁵ As shown in red in Figure 5, this mechanism involves the three-membered transition structure **TS-4/A**. The calculated barrier $(\Delta G^{\ddagger}_{298})$ is 25.2 kcal/mol, which is in excellent agreement with that determined experimentally (25.3 kcal/mol, Table 3). The Pd–CF₃ bond lengthens significantly in the transition state (by 0.26 Å) relative to the ground state, whereas the Pd–Ph bond

elongates only slightly (by 0.03 Å). This is consistent with previous proposals that Pd– CF_3 bond breaking is the major contributor to the overall barrier for Ph– CF_3 coupling at Pd^{II} centers.^{3a}

Scheme 2. Pathways for formation of PhCF₃.

We next examined concerted reductive elimination via a three-coordinate transition structure involving a monodentate D'BPF ligand (Scheme 2, b and Figure 5, blue pathway). Notably, this pathway has been implicated in the literature from Pd^{II}(Ph)(CF₃) complexes bearing the BrettPhos ligand. ¹³ DFT predicts that dissociation of one arm of D'BPF to form **B** is thermodynamically unfavorable ($\Delta G = +6.5 \text{ kcal/mol}$). The barrier for this dissociation is estimated from potential energy scans as $\Delta E^{\ddagger} \sim 10 \text{ kcal/mol}$). This is consistent with the dynamic behavior of **4** observed by NMR spectroscopy (Figure 3 and Scheme 1). However, concerted reductive elimination from **B** has a significantly higher barrier than that from the 4-coordinate species ($\Delta \Delta G^{\ddagger} = +5.9 \text{ kcal/mol}$, respectively). As such, the calculations suggest that this is not a competitive pathway to the formation of PhCF₃.

Finally, we explored the pathway involving C-F coupling from a Pd^{II} (difluorobenzyl)(fluoro) intermediate (Scheme 2, pathway c). Importantly, this pathway has been implicated in

our recent studies of Ph-CF₃ coupling from three-coordinate Pd^{II}(Ph)(CF₃) complexes of P'Bu₃⁸ and has also been calculated as a feasible pathway for (Xantphos)Pd(Ph)(CF₃). 15 As shown in black in Figure 5, this pathway starts with dissociation of one arm of D'BPF to form **B**. α-Fluoride elimination then occurs to generate the difluorocarbene intermediate D. Subsequent migratory insertion of the phenyl group into the Pd=CF₂ bond affords 3-coordinate complex E, which can traverse a very small barrier to give the four-coordinate analogue 5. Notably, the calculations indicate that 5 is 16 kcal/mol more stable than 4. Both E and 5 can participate in PhCF₂-F bond-forming reductive elimination, but reaction from the 3-coordinate complex has a higher transition state ($\Delta\Delta G^{\ddagger} = +2 \text{ kcal/mol}$). Overall, the highest energy transition structure along this pathway is that for the initial α-fluoride elimination (+26.4 kcal/mol). This is 1.2 kcal/mol higher than that for concerted Ph-CF₃ coupling from 4, suggesting that this is not the major pathway operating for complex 4.

We next examined analogous pathways for the DⁱPrPF complex **3** (Figure 6). In this system, concerted Ph–CF₃ coupling from the 4-coordinate complex (pathway a) has a calculated barrier of 33.6 kcal/mol. This is similar to that observed experimentally (31.4 kcal/mol, Table 3). The dissociation of one arm of the DⁱPrPF ligand to form a three-coordinate intermediate involves a large energetic penalty, as **B**ⁱ is 21.4 kcal/mol uphill from the starting material **3**. Furthermore, concerted Ph–CF₃ coupling from **B**ⁱ (pathway b) does not appear to be feasible in this system. Instead, all attempts to locate a transition structure for this reaction resulted in recoordination of the pendant phosphine arm.

Finally, the transition state for α -fluoride elimination from ${\bf B^i}$ (the first step of pathway c) is at 36.1 kcal/mol. This is 2.5 kcal/mol higher than that for concerted reductive elimination from ${\bf 3}$, suggesting that pathway c is unlikely to be a major contributor to the reactivity of the DⁱPrPF complex. Additionally, this step leads to a very stable 4-coordinate (DⁱPrPF)Pd(CF₂Ph)(F) complex ${\bf 6}$. This complex appears to be a thermodynamic sink in this system, as it is at considerably lower energy than both the starting material ${\bf 3}$ (-24.5 kcal/mol relative to ${\bf 3}$) and the reductive elimination product ${\bf F^i}$ (-15.9 kcal/mol relative to ${\bf F^i}$).

Overall, these calculations implicate concerted reductive elimination from the 4-coordinate starting materials as the major pathways for PhCF₃ formation in these systems. Additionally, they suggest that $Pd^{II}(CF_2Ph)(F)$ complexes should be stable species that can be independently isolated, characterized, and evaluated.

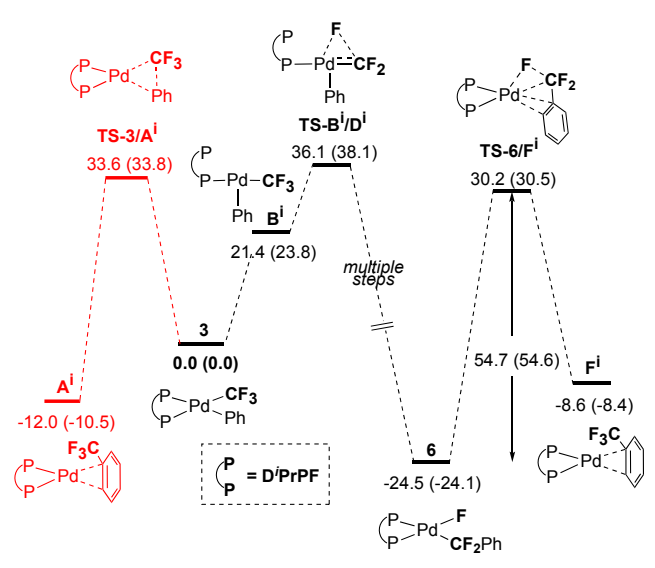


Figure 6. Energy profile for computed reactivity of $(D^i PrPF)Pd(Ph)(CF_3)$ (3), illustrating pathway a and key steps of pathway c (in black). Pathway b is not feasible in this system, as efforts to find a TS for Ph–CF₃ coupling from B^i led to recoordination of the phosphine ligand. A^i and F^i are conformers. Energies $\Delta G(\Delta H)$ in kcal/mol.

Synthesis of (D'PrPF)Pd^{II}(CF₂Ph)(F) (6). A final set of investigations focused on the synthesis and reactivity studies of (D'PrPF)Pd(CF₂Ph)(F) (6). As discussed above, such Pd^{II} difluorobenzyl fluoride intermediates have been proposed (but not detected or isolated) in other PhCF₃ couplings at Pd^{II} centers. 8,15 However, in the current system our calculations indicate that the barrier for PhF₂C-F coupling from 6 is >50 kcal/mol (Figure 6). Baker has recently shown that the reaction of Co^{III}– CF₃ complexes with trimethylsilyl trifluoromethanesulfonate (TMSOTf) results in the abstraction of a fluoride to yield trimethylsilyl fluoride (TMSF) and Co^{III}=CF₂⁺. ³⁷ We hypothesized that the treatment of 3 with TMSOTf would afford the difluorocarbene complex (7), which could undergo fast phenyl migration to produce (D'PrPF)Pd(CF₂Ph)(OTf) (8). The addition of CsF to 8 should then form product 6. Indeed, as summarized in Scheme 3, this reaction sequence yielded 6 in 50% isolated yield after recrystallization. Complex 6 was characterized by Xray crystallography (Figure 7) as well as ¹H, ¹⁹F, and ³¹P NMR spectroscopy.

Scheme 3. Independent synthesis of complex **6**.



Figure 7. ORTEP diagram for **6**. Hydrogen atoms have been omitted for clarity and ellipsoids are shown at 50% probability.

Studying the thermolysis of 6 required a change of solvent, as this complex is insoluble in *p*-xylene even at 130 °C. However, 6 does dissolve in *N*-methyl-2-pyrrolidone (NMP) after 5 min of heating at 130 °C. After heating at 130 °C for 2.25 h, no starting material remained as determined by ¹⁹F NMR spectroscopic analysis. Additionally, no trace of benzotrifluoride was detected, suggesting that 6 decomposes by unproductive pathways under these conditions (Scheme 4).³⁸ This result is consistent with the DFT calculations showing an extremely high barrier (54.7 kcal/mol) for PhF₂C–F bond-forming reductive elimination from 6.

Scheme 4. Thermolysis of complex **6**.

CONCLUSION

Phosphinoferrocenes (P~P) have been identified as an effective ligand scaffold for promoting Ph–CF₃ coupling from Pd^{II} centers. Systematic studies revealed that increasing the size of the phosphine substituents dramatically increases the rate of reductive elimination of PhCF₃. The mechanism of the reductive elimination to form PhCF₃ was explored computationally. The lowest energy pathway appears to involve concerted Ph–CF₃ bond-forming reductive elimination from four-coordinate

¹ (a) Ritter, T. Catalysis: fluorination made easier. *Nature* **2010**, 466, 447-448. (b) Lundgren, R. J.; Stradiotto, M. Transition-metal-catalyzed trifluoromethylation of aryl halides. Angew. Chem. Int. Ed. 2010, 49, 9322-9324. (c) Furuya, T.; Kamlet, A. S.; Ritter, T. Catalysis for fluorination and trifluoromethylation. Nature 2011, 473, 470-477. (d) Tomashenko, O. A.; Grushin, V. V. Aromatic trifluoromethylation with metal complexes. Chem. Rev. 2011, 111, 4475-4521. (e) Chen, P.; Liu, G. Recent advances in transition-metal-catalyzed trifluoromethylation and related transformations. Synthesis 2013, 45, 2919-2939. (f) Landelle, G.; Panossian, A.; Pazenok, S.; Vors, J.-P.; Leroux, F. R. Recent advances in transition metal-catalyzed Csp²-monofluoro-, difluoro-, perfluoromethylation and trifluoromethylthiolation. Beilstein J. Org. Chem. 2013, 9, 2476-2536. (g) Zhu, W.; Wang, J.; Wang, S.; Gu, Z.; Aceña, J. L.; Izawa, K.; Liu, H.; Soloshonok, V. A. Recent advances in the trifluoromethylation methodology and new CF₃-containing drugs. J. Fluorine Chem. 2014. 167. 37-54. (h) Alonso, C.: Martínez de Marigorta, E.; Rubiales, G.; Palacios, F. Carbon trifluoromethylation reactions of hydrocarbon derivatives and heteroarenes. Chem. Rev. 2015, 115, 1847-1935.

² For selected examples, see: (a) Oishi, M.; Kondo, H.; Amii, H. Aromatic trifluoromethylation catalytic in copper. *Chem. Commun.* **2009**, 1909-1911. (b) Knauber, T.; Arikan, F.; Röschenthaler, G.-V.; Gooßen,

 $(P\sim P)Pd(Ph)(CF_3)$ complexes. There is excellent agreement between experimental and DFT-derived activation parameters for this pathway. Reductive elimination from a three-coordinate complex, formed upon dissociation of one arm of the bidentate ligand, is a higher energy pathway in all cases examined. Additionally, DFT analysis suggests that pathways involving α -fluoride elimination are not competitive in these systems. This prediction was validated through the synthesis of (Di-PrPF)Pd(CF₂Ph)(F) and the demonstration that this complex does not form PhCF₃ upon thermolysis at temperatures up to 130 °C. Overall, the results of these studies are consistent with many of the computational findings of Schoenebeck¹⁴ as well as Bakhmutov, Grushin, and Macgregor. 15 Specifically, they show experimentally that the use of sterically large and wide bite angle bidentate phosphine ligands can be highly effective for promoting Ph–CF₃ bond forming reductive elimination from PdII centers.

ASSOCIATED CONTENT

Supporting Information

AUTHOR INFORMATION

Corresponding Author

* mssanfor@umich.edu

ORCID

Melanie S. Sanford: 0000-0001-9342-9436

Allan J. Canty: 0000-0003-4091-6040

ACKNOWLEDGMENT

This work was supported by the National Science Foundation (CHE-1664961 and CHE-0840456 for X-ray instrumentation). We thank Dr. Christo Sevov for valuable discussions. The authors declare no competing financial interests.

REFERENCES

L. J. Copper-catalyzed trifluoromethylation of aryl iodides with potassium (trifluoromethyl)trimethoxyborate. Chem. Eur. J. 2011, 17, 2689-2697. (c) Li, Y.; Chen, T.; Wang, H.; Zhang, R.; Jin, K.; Wang, X.; Duan, C. A ligand-free copper-catalyzed decarboxylative trifluoromethylation of aryl iodides with sodium trifluoroacetate using Ag₂O as a promoter. Synlett 2011, 1713-1716. (d) Kondo, H.; Oishi, M.; Fujikawa, K.; Amii, H. Copper-catalyzed aromatic trifluoromethylation via group transfer from fluoral derivatives. Adv. Synth. Catal. 2011, 353, 1247-1252. (e) Weng, Z.; Lee, R.; Jia, W.; Yuan, Y.; Wang, W.; Feng, X.; Huang, K.-W. Cooperative effect of silver in copper-catalyzed trifluoromethylation of aryl iodides using Me₃SiCF₃. Organometallics 2011, 30, 3229-3232. (f) Schareina, T.; Wu, X.-F.; Zapf, A.; Cotté, A.; Gotta, M.; Beller, M. Towards a practical and efficient copper-catalyzed trifluoromethylation of aryl halides. Top. Catal. 2012, 55, 426-431. (g) Nakamura, Y.; Fujiu, M.; Murase, T.; Itoh, Y.; Serizawa, H.; Aikawa, K.; Mikami, K. Cu-catalyzed trifluoromethylation of aryl iodides with trifluoromethylzinc reagent prepared in situ from trifluoromethyl iodide. Beilstein J. Org. Chem. 2013, 9, 2404-2409. (h) Gonda, Z.; Kovács, S.; Wéber, C.; Gáti, T.; Mészáros, A.; Kotschy, A.; Novák, Z. Efficient copper-catalyzed trifluoromethylation of aromatic and heteroaromatic iodides: the beneficial anchoring effect of borates. Org. Lett. 2014, 16, 4268-4271. (i) Zhao, S.; Guo, Y.; Han, E.-J.; Luo,

- J.; Liu, H.-M.; Liu, C.; Xie, W.; Zhang, W.; Wang, M. Copper(II)-catalyzed trifluoromethylation of iodoarenes using Chen's reagent. *Org. Chem. Front.* **2018**, *5*, 1143-1147. (j) Le, C.; Chen, T.-Q.; Liang, T.; Zhang, P.; MacMillan, D. W. C. A radical approach to the copper oxidative addition problem: trifluoromethylation of bromoarenes. *Science* **2018**, *360*, 1010-1014.
- ³ (a) Cho, E. J.; Senecal, T. D.; Kinzel, T.; Zhang, Y.; Watson, D. A.; Buchwald, S. L. The palladium-catalyzed trifluoromethylation of aryl chlorides. *Science* **2010**, *328*, 1679-1681. (b) Samant, B. S.; Kabalka, G. W. A novel catalytic process for trifluoromethylation of bromoaromatic compounds. *Chem. Commun.* **2011**, *47*, 7236-7238. (c) Martínez de Salinas, S.; Mudarra, Á. L.; Benet-Buchholz, J.; Parella, T.; Maseras, F.; Pérez-Temprano, M. H. New vistas in transmetalation with discrete "AgCF₃" species: implications in Pd-mediated trifluoromethylation reactions. *Chem. Eur. J.* **2018**, *24*, 11895-11898.
- ⁴ Aroyl fluorides have been transformed into trifluoromethyl arenes using Pd catalysis, see: Keaveney, S. T.; Schoenebeck, F. Palladium-catalyzed decarbonylative trifluoromethylation of acid fluorides. *Angew. Chem. Int. Ed.* **2018**, *57*, 4073-4077.
- ⁵ Grushin, V. V.; Marshall, W. J. Facile Ar-CF₃ bond formation at Pd. Strikingly different outcomes of reductive elimination from [(Ph₃P)₂Pd(CF₃)Ph] and [(Xantphos)Pd(CF₃)Ph]. *J. Am. Chem. Soc.* **2006**, *128*, 12644-12645.
- ⁶ Nielsen, M. C.; Bonney, K. J.; Schoenebeck, F. Computational ligand design for the reductive elimination of ArCF₃ from a small bite angle Pd^{II} complex: remarkable effect of a perfluoroalkyl phosphine. *Angew. Chem. Int. Ed.* **2014**, *53*, 5903-5906.
- ⁷ Maleckis, A.; Sanford, M. S. Catalytic cycle for palladium-catalyzed decarbonylative trifluoromethylation using trifluoroacetic esters as the CF₃ source. *Organometallics* **2014**, *33*, 2653-2660.
- ⁸ Ferguson, D. M.; Bour, J. R.; Canty, A. J.; Kampf, J. W.; Sanford, M. S. Stoichiometric and catalytic aryl-perfluoroalkyl coupling at tritert-butylphosphine palladium(II) complexes. *J. Am. Chem. Soc.* **2017**, *139*, 11662-11665.
- ⁹ (a) Brown, J. M.; Guiry, P. J. Bite angle dependence on the rate of reductive elimination from diphosphine palladium complexes. *Inorg. Chim. Acta* **1994**, *220*, 249-259. (b) Marcone, J. E.; Moloy, K. G. Kinetic study of reductive elimination from the complexes (diphosphine)Pd(R)(CN). *J. Am. Chem. Soc.* **1998**, *120*, 8527-8528.
- ¹⁰ Sterically hindering and electron withdrawing ligands are known to promote reductive elimination from Pd^{II}, see: Hartwig, J. F. Electronic effects on reductive elimination to form carbon-carbon and carbon-heteroatom bonds from palladium(II) complexes. *Inorg. Chem.* **2007**, *46*, 1936-1947.
- ¹¹ For theoretical investigations of reductive elimination from Pd^{II}, see: (a) Tatsumi, K.; Hoffmann, R.; Yamamoto, A.; Stille, J. K. Reductive elimination of d⁸-organotransition metal complexes. *Bull. Chem. Soc. Jpn.* **1981**, *54*, 1857-1867. (b) Ananikov, V. P.; Musaev, D. G.; Morokuma, K. Critical effect of phosphine ligands on the mechanism of carbon-carbon bond formation involving palladium(II) complexes: a theoretical investigation of reductive elimination from square-planar and t-shaped species. *Eur. J. Inorg. Chem.* **2007**, 5390-5399. (c) Pérez-Rodríguez, M.; Braga, A. A. C.; Garcia-Melchor, M.; Pérez-Temprano, M. H.; Casares, J. A.; Ujaque, G.; de Lera, A. R.; Álvarez, R.; Maseras, F.; Espinet, P. C-C reductive elimination in palladium complexes, and the role of coupling additives. A DFT study supported by experiment. *J. Am. Chem. Soc.* **2009**, *131*, 3650-3657.
- ¹² For an experimental example comparing 3-coordinate and 4-coordinate reductive elimination from Pd^{II}, see: Yamashita, M.; Hartwig, J. F. Synthesis, structure, and reductive elimination chemistry of three-coordinate arylpalladium amido complexes. *J. Am. Chem. Soc.* **2004**, *126*, 5344-5345.
- ¹³ Zhang, S.-L.; Huang, L.; Sun, L.-J. The mechanism, electronic and ligand effects for reductive elimination from arylPd(II)trifluoromethyl complexes: a systematic DFT study. *Dalton Trans.* **2015**, *44*, 4613-4622.
- ¹⁴ Anstaett, P.; Schoenebeck, F. Reductive Elimination of ArCF₃ from Bidentate Pd^{II} Complexes: A Computational Study. *Chem. Eur. J.* **2011**, *17*, 12340-12346.
- ¹⁵ Bakhmutov, V. I.; Bozoglian, F.; Gómez, K.; González, G.; Grushin, V. V.; Macgregor, S. A.; Martin, E.; Miloserdov, F. M.;

- Novikov, M. A.; Panetier, J. A.; Romashov, L. V. CF₃-Ph reductive elimination from [(Xantphos)Pd(CF₃)(Ph)]. *Organometallics* **2012**, *31*, 1315-1328.
- ¹⁶ (a) Driver, M. S.; Hartwig, J. F. A second-generation catalyst for aryl halide amination: mixed secondary amines from aryl halides and primary amines catalyzed by (DPPF)PdCl₂. *J. Am. Chem. Soc.* **1996**, *118*, 7217-7218. (b) Hamann, B. C.; Hartwig, J. F. Systematic variation of bidentate ligands used in aryl halide amination. Unexpected effects of steric, electronic, and geometric perturbations. *J. Am. Chem. Soc.* **1998**, *120*, 3694-3703.
- ¹⁷ Mann, G.; Shelby, Q.; Roy, A. H.; Hartwig, J. F. Electronic and steric effects on the reductive elimination of diaryl ethers from palladium(II). *Organometallics* **2003**, *22*, 2775-2789.
- ¹⁸ This method has been used for the synthesis of (DPPF)Pd^{II}(Ar)(CF₂H) complexes, see: Gu, Y.; Leng, X.; Shen, Q. Cooperative dual palladium/silver catalyst for direct difluoromethylation of aryl bromides and iodides. *Nat. Commun.* **2014**, *5*, 5405.
- ¹⁹ Spessard, G. O.; Miessler, G. L. Organometallic Reactions I: Reactions That Occur at the Metal. *Organometallic Chemistry*, 2nd Ed.; Oxford University Press, Inc.: New York, 2010; pp 179-181.
- ²⁰ This distortion was observed in a related complex (see ref 17) and in (Xantphos)Pd^{II}(Ph)(CF₃) (see ref 15).
- ²¹ Based on a search of the Cambridge Structural Database (CSD) Version 5.39, updated August 2018. General citation: Groom, C. R.; Bruno, I. J.; Lightfoot, M. P.; Ward, S. C. *Acta Cryst. Sect. B: Struct. Sci., Cryst. Eng. Mater.* **2016**, *72*, 171-179.
- ²² (Xantphos)Pd^{II}(Ph)(CF₃) displays similar fluxional behavior in solution, see refs 5 and 15.
- ²³ An alternative mechanism was proposed for the isomerization of (Xantphos)Pd^{II}(Ph)(CF₃) that does not involve phosphine dissociation. Rather, the transition state adopts a "truncated trigonal bipyramidal structure" in which the CF₃ ligand is in an equatorial plane with the phosphine ligands and the phenyl ligand in an axial coordination site. See ref 15. Due to the sterics of D'BPF and the long Pd–P1 bond length (2.5639 Å) observed in the solid-state structure of 4, we propose the ligand dissociation pathway as described in Scheme 1.
- ²⁴ The addition of phosphine to trap Pd⁰ products is common in studies of reductive elimination from Pd^{II} centers. For an example, see ref 17.
- ²⁵ The major Pd species observed after the reductive elimination with D'BPF complex **4** was D'BPF ligated Pd⁰ species as identified by ³¹P NMR and no formation of Pd black was observed.
- ²⁶ (Xantphos)Pd(Ph)(CF₃) was found to afford PhCF₃ in quantitative yield after heating at 80 °C for 3 h, see ref 5 and 15.
- $^{27}\,D'BPF$ did not afford Ar–CF3 under $Pd^{0/II}$ -catalysis conditions. See the Supporting Information for details. We tentatively propose that large size of D'BPF may hinder transmetallation in this catalytic system.
- ²⁸ Thermolysis of **4** in the absence of added phosphine ligand under otherwise identical conditions afforded full conversion of **4** and 55% PhCF₃ as determined by ¹⁹F NMR spectroscopy.
- 29 Bakhmutov, Grushin, and Macgregor experimentally determined that (Xantphos)Pd(Ph)(CF₃) undergoes reductive elimination with ΔH^{\ddagger} = 25.9 kcal/mol and ΔS^{\ddagger} = 6.4 eu (see ref 15), suggesting that (D'BPF)Pd(Ph)(CF₃) and (Xantphos)Pd(Ph)(CF₃) have comparable activation parameters for reductive elimination.
- ³⁰ Gaussian 09 was used at the M06 (ref 31) level for geometry optimization. The Stuttgart/Dresden ECP (SDD) was used to describe Pd and Fe (ref 32), and the 6-31G(d) basis set was used for other atoms to form basis set BS1. All computation was carried out for benzene as the solvent utilizing the IEFPCM (SCRF) model. Single point calculations were performed at the B3LYP-D3 level, as recent studies indicate that the D3 calculation is suitable in accounting for dispersion (ref 33), including for related palladium phosphine systems (ref 34). These calculations employed the quadrupole-ξ valence polarized def2-QZVP (ref 35) basis set on Pd and Fe along with the corresponding ECP and the 6-311+G(2d,p) basis set on other atoms (basis set BS2). All thermodynamic data were calculated at the standard state (298.15 K and 1 atm). To estimate the corresponding Gibbs free energies in benzene (ΔG), entropy corrections were calculated at the M06/BS1 level and added to the single point potential energies. All transition structures contained

one imaginary frequency, exhibiting atom displacements consistent with the anticipated reaction pathway. The nature of transition structures was confirmed by intrinsic reaction coordinate (IRC) searches, vibrational frequency calculations, and potential energy surface scans. Natural charge population analyses were performed in conjunction with BS1 (ref 36).

³¹ (a) Zhao, Y.; Schultz, N. E.; Truhlar, D. G. Design of density functionals by combining the method of constraint satisfaction with parameterization for thermochemistry, thermochemical, kinetics, and noncovalent interactions. *J. Chem. Theory Comput.* **2006**, *2*, 364-382. (b) Zhao, Y.; Truhlar, D. G. A new local density functional for main-group thermochemistry, transition metal bonding, thermochemical kinetics, and noncovalent interactions. *J. Chem. Phys.* **2006**, *125*, 194101. (c) Zhao, Y.; Truhlar, D. G. Density functional for spectroscopy: no longrange self-interaction error, good performance for Rydberg and charge-transfer states, and better performance on average than B3LYP for ground states. *J. Phys. Chem. A* **2006**, *110*, 13126-13130. (d) Zhao, Y.; Truhlar, D. G. Density functionals with broad applicability in chemistry. *Acc. Chem. Res.* **2008**, *41*, 157-167.

³² Andrae, H.; Häußermann, U.; Dolg, M.; Stoll, H.; Preuß, H. Energy-adjusted ab initio pseudopotentials for the second and third row transition elements. *Theor. Chim. Acta* **1990**, *77*, 123-141.

³³ (a) Ehrlich, S.; Moellmann, J.; Grimme, S. Dispersion-corrected density functional theory for aromatic interactions in complex systems.

Acc. Chem. Res. **2013**, *46*, 916-926. (b) Antony, J.; Sure, R.; Grimme, S. Using dispersion-corrected density functional theory to understand supramolecular binding thermodynamics. *Chem. Commun.* **2015**, *51*, 1764-1774.

³⁴ Lyngvi, E.; Sanhueza, I. A.; Schoenebeck, F. Dispersion makes the difference: bisligated transition states found for the oxidative addition of Pd(PtBu₃)₂ to Ar-OSO₂R and dispersion-controlled chemoselectivity in reactions with Pd[P(iPr)(tBu)₂)₂. *Organometallics* **2015**, *34*, 805-812.

³⁵ Weigend, F.; Furche, F.; Ahlrichs, R. Gaussian basis sets of quadruple zeta valence quality for atoms H-Kr. *J. Chem. Phys.* **2003**, *119*, 12753-12762.

³⁶ Glendening, E. D.; Read, A. E.; Carpenter, J.E.; Weinhold, F. *NBO*, version 3.1; Gaussian Inc.; Pittsburgh, PA, 2003.

³⁷ Lecler, M. C.; Bayne, J. M.; Lee, G. M.; Gorelsky, S. I.; Vasiliu, M.; Korobkov, I.; Harrison, D. J.; Dixon, D. A.; Baker, R. T. Perfluoro-alkyl cobalt(III) fluoride and bis(perfluoroalkyl) complexes: catalytic fluorination and selective difluorocarbene formation. *J. Am. Chem. Soc.* **2015**, *137*, 16064-16073.

³⁸ Heating **3** for 24 h under analogous conditions afforded PhCF₃ in 58% yield with 69% conversion of **3**.